Experimental analysis of flow boiling heat transfer in multi-microchannel evaporators

Experimental analysis of flow boiling heat transfer in multi-microchannel evaporators

F Riccardi[1], G Zummo[2,*], L Saraceno[2], L Gugliermetti[2], G Caruso[1]

[1] Dep. of Astronautical Electrical and Energy Engineering (DIAEE)
NERG - Nuclear Engineering Research Group, Corso Vittorio Emanuele II, 244, 00186 Rome (Italy)

[2] ENEA C.R. Casaccia
Laboratory of Processes and Systems Engineering for Energy Decarbonisation, Via Anguillarese, 301, 00123 Rome (Italy)

[*] Corrisponding author: giuseppe.zummo@enea.it

Abstract. This paper provides an experimental analysis of flow boiling heat transfer in four finned evaporators with different aspect ratio and heated length have been tested. R245fa was the refrigerant chosen as working fluid for its good thermal characteristics. The imposed heat flux at the footprint covered a range from 30 to 330 kW/m^2, while the fluid mass fluxes within the channel varied in a range between 17 and 225 kg/m^2 s. The hydraulic diameters of the investigated evaporators were 1.15 mm and 2.09 mm, with aspect ratio (channel width/channel height) respectively of 0.3 and 0.72. Thanks to the measuring apparatus, heat transfer data were collected and then processed to calculate the local heat transfer coefficients, using the fin array heat transfer model. These local values of the heat transfer coefficient were then compared with those calculated from existing correlations for mini-micro channels flow boiling and the Mean Absolute Percent Error was finally assessed.

1. Introduction

In recent years, given the trend toward miniaturization of components and simultaneous increase in their performance, the use of mini-microchannel heat sinks has been of great interest to cope with the increased heat fluxes and to ensure an adequate thermal control of the components where they are installed.

There are many applications of this technology in several industrial fields such as the cooling of electronic power converters for electric vehicles, but also next-generation microprocessors such as Data Centres' CPUs and GPUs, whose cooling process is to date an extremely energy-intensive activity.

IGBT (Insulated-Gate Bipolar Transistor) modules for electric vehicles represent an example of high-heat flux electrical component and they are widely used inside electrical vehicles inverters and charging stations. They generate heat fluxes in the range from 6.5 to 50 MW/m^2(based on the die size of the chip [1]). These devices should be maintained at a temperature lower than 100-115°C to avoid early failures, while , in the ICT (Information and Communication Technology) field the threshold temperature of the processors is set around 80-85°C. In 2007 Yang et al. [2] found that the CPU's processing speed is severely affected by the chip temperature decreasing by 10-15% only due to local temperature surges, which may exceed by 30°C the average chip temperature. Using organic refrigerants with saturation temperature at operative pressure lower than the threshold value imposed for the correct operation of the devices, it is possible to combine the advantages of micro-channel heat sinks with those of the two-phase heat transfer, such as the temperature uniformity above the cooled surfaces and the enhanced heat transfer coefficient due to the evaporation process, reducing the required pumping power, with respect to an equivalent single-phase

cooling system. The major drawback of this technology is the high degree of complexity. Furthermore, in this kind of heat sinks the heat flux decreases steadily with increasing distance from the base and the top side of channel is an unheated surface. Since the two-phase heat transfer coefficient is heat-flux dependent, this unevenness in the heating condition strongly affects the heat transfer mechanism. A very comprehensive review of the various transition criteria and of the main issues concerning microchannel flow-boiling was conducted by Mahmoud and Karayiannis in 2017 [1].

In 2022 Criscuolo et al. [3] studied the flow boiling of R1234yf, R1234ze(E), R134a finding that the boiling development in high aspect ratio micro-channels can be divided in three regimes. In the first one the heat transfer coefficient is only determined by the heat flux, regardless of the mass flux. In the second one both the heat flux and the mass flux have an influence on the heat transfer coefficient, due to the superimposition of the nucleation and forced convection heat transfer mechanisms. The last regime is the one in which occurs the dry-out of the channel and the heat transfer coefficient rapidly drops. In 2016 Gugliermetti et al. [4] studied the saturated flow boiling of FC-72 in a 1 mm tube, testing several correlations for the heat transfer coefficient. The best result was obtained with the Li and Wu correlation for micro-channels.

2. Experimental test rig and measurement uncertainty

2.1 Experimental plant and fluid loops

The experimental facility is provided by the Casaccia research centre of ENEA (Agenzia Nazionale per le Nuove Tecnologie, l'Energia e lo Sviluppo Economico Sostenibile). The whole experimental system mainly consists of two fluid circuits: a primary circuit filled with the coolant and a secondary circuit for the cooling water. There is also a third loop, with a fan coil cooler to dissipate excess heat. A simplified diagram of the experimental setup is showed in Figure 1.

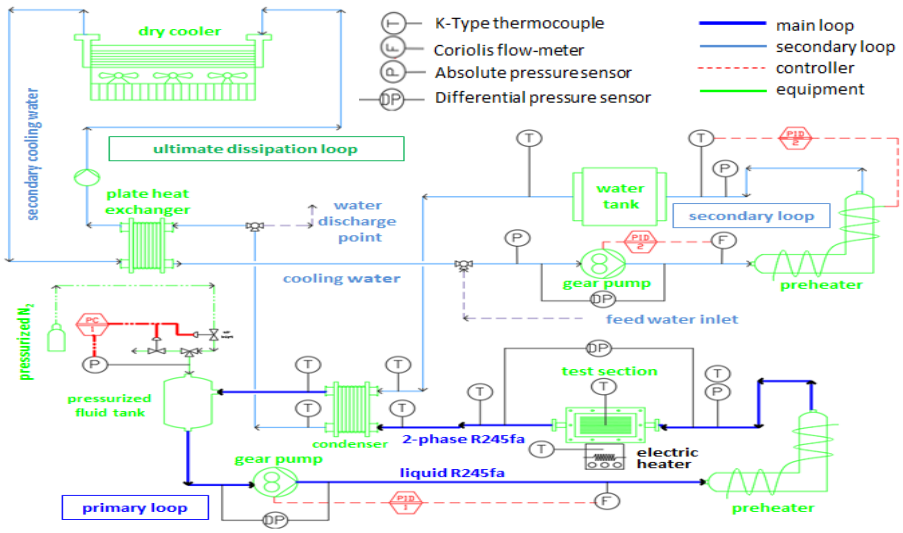

Figure 1. Piping and Instrumentation Diagram of the experimental plant

Liquid refrigerant is circulated by means of a gear- pump. The tank is placed in the upper part of the loop, to guarantee an adequate suction head avoiding pump cavitation. The pressure inside the tank is regulated by a solenoid valve that injects and expels N_2. Before entering the multichannel-evaporator (with a sub cooling varying between 5 and 20 °C), the liquid flow rate is measured by a Coriolis flowmeter. Two K-type thermocouples are placed at the evaporator inlet and outlet sleeves to measure the fluid bulk temperatures. An absolute pressure transducer is placed at the inlet of the evaporator, while the pressure drops across the test section are measured with a differential pressure sensor. The evaporator footprint temperatures are measured by means of calibrated K-type thermocouples inserted in the metallic base. The

input heat-rate is provided by three cartridge heaters (400W) each, placed inside an aluminium cube, to simulate the surface of the chip to be cooled. The temperature of this surface is measured by a thermocouple inserted in a hole on the top of the aluminium block. Once evaporated, the fluid is condensed in a plate heat exchanger, cooled by the water coming from the secondary loop. Then, the condensed fluid finally returns to the storage tank.

2.2 Test section

The test section consists of the aluminium multichannel evaporator covered with a polycarbonate cover, the heating block, the instrumented inlet and outlet fluid sleeves, and the thermocouples to measure the wall temperatures. The whole heated part is insulated with low conductivity bricks made of vermiculite (~ 0.10 W/m°C), to reduce thermal losses. Figure 2 shows the evaporator with all its main dimensions

Main Dimensions	*E50*	*E50-2*	*A100*	*A100-2*
Channel's width	0.75	1.8	1.8	0.75
Channel's height	2.5	2.5	2.5	2.5
Hydraulic diameter	1.15	2.09	2.09	1.15
Channel's length	50	50	100	100
Fin thickness	0.3	0.5	0.5	0.3

Figure 2. Evaporator and main dimensions in *mm*.

3. Method

The real-time acquisition of all measured variables is achieved by means of a program developed in LabVIEW, within which are also set safety thresholds for maximum operating pressure, minimum flow rate, and maximum temperatures. Beyond these threshold values the power supply is cut off by the system. The same program also allows to control the flow rate, pressure, and power during the tests.

The measured quantities are acquired at a frequency of 1000 Hz and the program automatically calculates the average value recording one line containing these stored averages each second. Acquisition occurs only when surface temperatures have stabilized, and their standard deviation is low.

4. Data reduction

The collected data are then analysed using Python scripts and Excel spreadsheets, while the thermodynamic quantities are calculated using REFPROP 10 software, developed by NIST [5].

Below it is reported a summary of the calculations performed.

To get rid of the channel dimension and to consider the flow velocity within it, the mass flux has been calculated as the ratio between the mass flow rate $\dot{m}$ and the transversal flow area A_{flow}.

By heating the evaporators in vacuum conditions and waiting for steady temperatures, the heat losses towards the external environment have been calculated and the net heat rate is then calculated as the difference between the measured input power and the calculated heat losses.

To consider the actual position of the inserted thermocouples inside the channel, the dimensionless axial position ($\tilde{z}_{ad_i}$) has been calculated as the ratio between the axial coordinate of the relative thermocouple z_i and the channel length L_{ch}. Thermodynamic equilibrium quality is obtained from its definition, knowing the mixture enthalpy by the energy balance.

$$x_i = \frac{h_{in} - h_f}{h_{fg}} + \tilde{z}_{ad_i} \cdot \frac{\dot{q}_{net}}{h_{fg} \cdot \dot{m}} \tag{1}$$

From the assumption of uniform power distribution over the heater surface, it follows that the bulk temperature of the fluid linearly increases along the channel until saturation is reached. The quality has been used as reference value to calculate the real bulk temperature T_{∞_i} .

$$T_{\infty_i} = T_{sat} \ (x_i \geq 0) \qquad ; \qquad T_{\infty_i} = \tilde{z}_{ad_i} \cdot \frac{\dot{q}_{net}}{\dot{m}\, c_p} + T_{in} \ (x_i < 0) \tag{2}$$

The Fourier law of conductive heat transfer has been applied to get the temperature of the channel's base in contact with the fluid starting from the measured temperature of the bottom surface.

The ΔT used to calculate the heat transfer coefficient in boiling condition, has been calculated as the difference between the temperature of channel's base and that of the fluid bulk. Due to the non –uniformity of the heat flux in vertical walls, the heat flux at the channel's footprint ($q"_{fp}$) is taken as reference and is calculated as the ratio between the net input power and the footprint area (A_{fp}) of the multichannel array. The fin model has been applied to consider the heat transferred by the vertical walls, and the fin efficiency has been calculated imposing adiabatic boundary conditions at the top (equation 3).

$$\eta_{fin} = \frac{\tanh\,(m \cdot H_{ch})}{m \cdot H_{ch}} \qquad \text{where:} \quad m = \sqrt{\frac{2 \cdot htc}{k_{material} \cdot s_{fin}}} \tag{3}$$

The heat transfer coefficient is also involved in the expression of the fin efficiency and for this reason an iterative procedure has been performed for its calculation, solving the thermal balance of the fin array.

The heated surface has been divided into the finned part and the remaining base surface which is exposed to the fluid. The formula can be rearranged into a more suitable form for iterative computation of the heat transfer coefficient htc, whose value has been calculated by solving the following non-linear equation 4:

$$\frac{\dot{q}_{net}}{\left(A_{exposed\ base\ ch} + \eta_{fin}(htc) \cdot A_{finned}\right) \cdot \Delta T_{wall\ i}} - htc = 0 \tag{4}$$

The first term in the previous equation represents the heat transfer coefficient calculated from Newton's law, imposing the heat flux corrected with the fin efficiency.

5. Uncertainties

The average uncertainty over measured quantities was calculated using the root sum of squares formula. The statistic component was assumed to follow a Gaussian distribution with coverage factor of 95% being twice the standard deviation. The propagation of uncertainty on calculated quantities, such as the heat flux has been estimated using equation 5. The average values of the uncertainty were reported in Table 1.

$$u_y = \sqrt{\left[(dy/dx_1) \cdot u_{x_1}\right]^2 + \cdots + \left[(dy/dx_n) \cdot u_{x_n}\right]^2} \tag{5}$$

Table 1. Average uncertainty on measured and computed quantities

Quantities	*E50*	*E50-2*	*A100*	*A100-2*	*Units*
Twall	± 0.13	± 0.12	± 0.562	± 0.575	°C
Psat	± 0.075	± 0.075	± 0.05	± 0.05	bar
Mass flow rate	± 0.079	± 0.0783	± 0.13	± 0.2	Kg/h
Net heat flux at the footprint	± 0.07%	± 0.06%	± 1.5%	± 1.5%	W/m^2

6. Experimental Results

The evaporators E50 and E50-2 were tested at different working pressures of 2 and 3 (T_{sat} equal to 34 and 46°C, respectively) and at three different mass fluxes of 64, 94 and 122 kg/m^{2}s. Results are graphically shown in the curves below (Figure 3), which show how in the evaporator with smaller hydraulic diameter, the heat transfer coefficient (at the centreline) reaches a maximum value, then tends to decrease with the

quality. The peak value of the htc increases with the pressure and slightly with the mass flux. This is due to the reduction of the specific volume of the vapour phase with increasing pressure, and thus, to the lower void fraction inside the channel (at equal quality). This leads to a lesser suppression of the nucleation mechanism which, instead, is slightly promoted by the reduction of latent heat. The decreasing arc of the curves is related to the nucleate boiling dominant stage of boiling, as reported also in the study carried out by Cheng et al. [6]. Moreover, it can be noticed that in the evaporator with wider channels the htc reaches values higher than in the other cases and it monotonically increases with the quality with a gradually decreasing slope. In the subcooled region, the heat transfer coefficient is almost not affected by the mass flux, because the fluid flow at the channel inlet is in laminar condition, with Nu number which tends to be constant (when fully developed). This is consistent with the three stages of boiling highlighted in the study of Criscuolo et al [3] and confirmed experimentally in the present study.

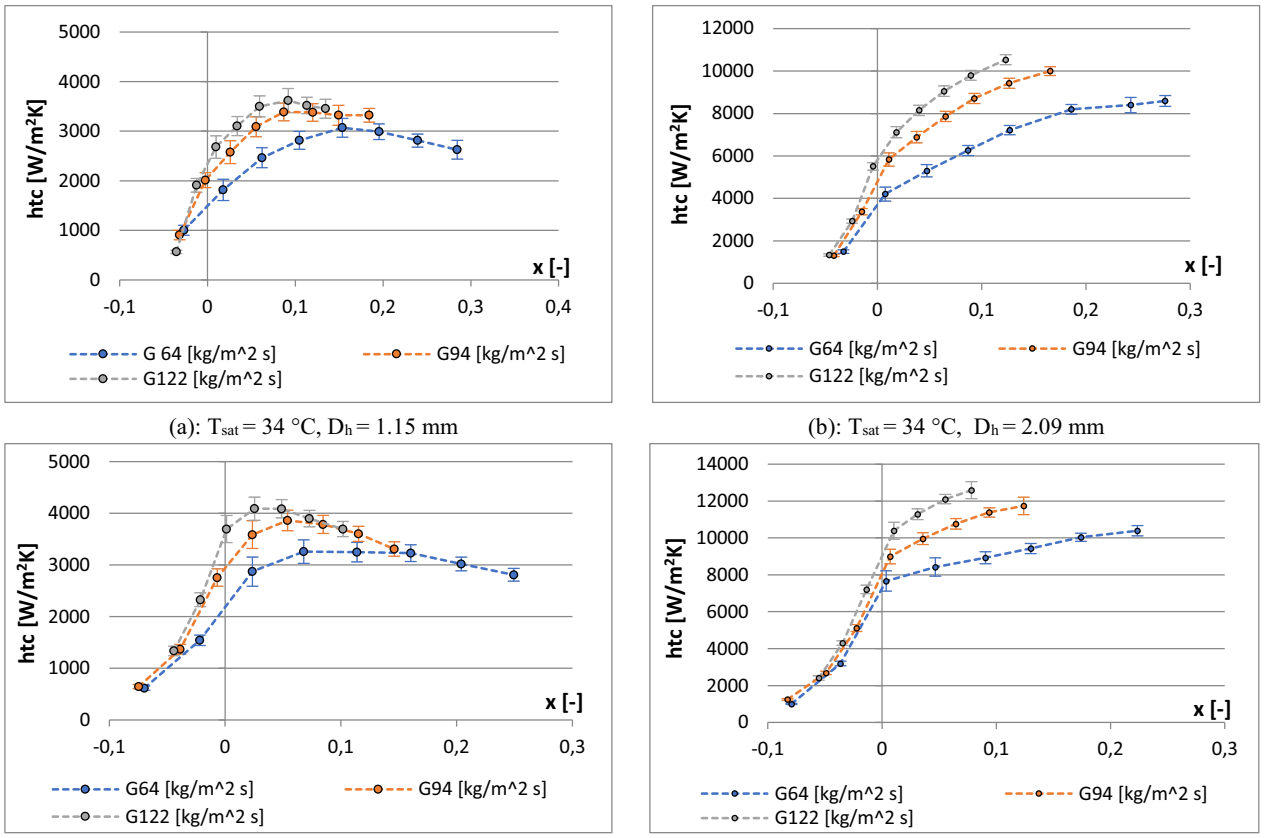

(a): T_{sat} = 34 °C, D_h = 1.15 mm

(b): T_{sat} = 34 °C, D_h = 2.09 mm

(c): T_{sat} = 46 °C, D_h = 1.15 mm

(d): T_{sat} = 46 °C, D_h = 2.09 mm

Figure 3. Experimental heat transfer coefficient as function of the local quality. L_{ch}=50 mm; $\tilde{x}_{ad_i}$= 0.5

The evaporators A100 and A100-2, with larger heated lengths have been tested with a working pressure of 1.8 bar (T_{sat} = 30.3 °C) and with different mass fluxes (32, 64, 97 and 128 kg/m^{2}s). In this case the htc has been measured near the channel outlet, at the dimensionless axial position of 0.87 and for this reason there are no experimental points in the subcooled region. At high heat fluxes, the heat transfer coefficient rapidly drops due to the incipience of the dry-out phenomenon, especially for the evaporator with a smaller channel diameter, as shown in Figure 4.

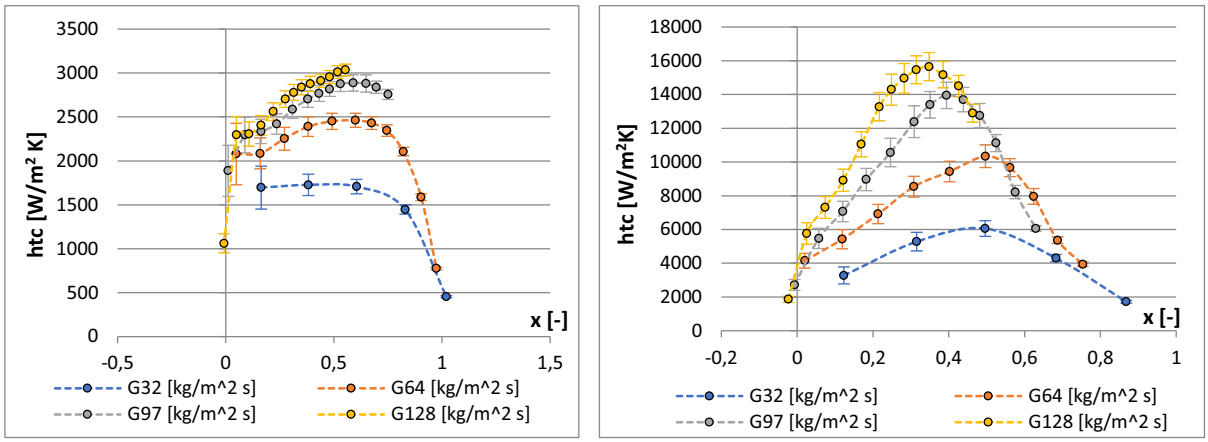

(c): T_{sat} = 30.3 °C, D_h = 1.15 mm (d): T_{sat} = 30.3 °C, D_h = 2.09 mm

Figure 4. Experimental heat transfer coefficient as function of local quality. L_{ch}=100 mm; $\tilde{x}_{di}$= 0.87.

7. Comparison with available correlations

The experimental htc has been also compared to the one calculated from available correlations developed for mini and micro-channels to verify their applicability to the measured data. The Mean Absolute Percent Error (MAPE), reported in Table 2, has been used to find out the correlation which gives better results in the tested range of heat and mass fluxes. The parity-plot diagrams have been developed and the most representative are shown in Figure 5. The heat transfer coefficient obtained from correlations developed for rectangular channels and small tubes with the whole perimeter heated has been multiplied by a factor Nu_3 / Nu_4 as done by Lee and Mudawar in [11].Where Nu_3 and Nu_4 are the laminar fully developed Nusselt numbers for a rectangular channel with respectively three and four heated walls. This coefficient is useful to estimate the effect of having only three heated walls during the htc calculations.

The tested correlations have been developed for small circular ducts or rectangular channels, with uniform heat flux.

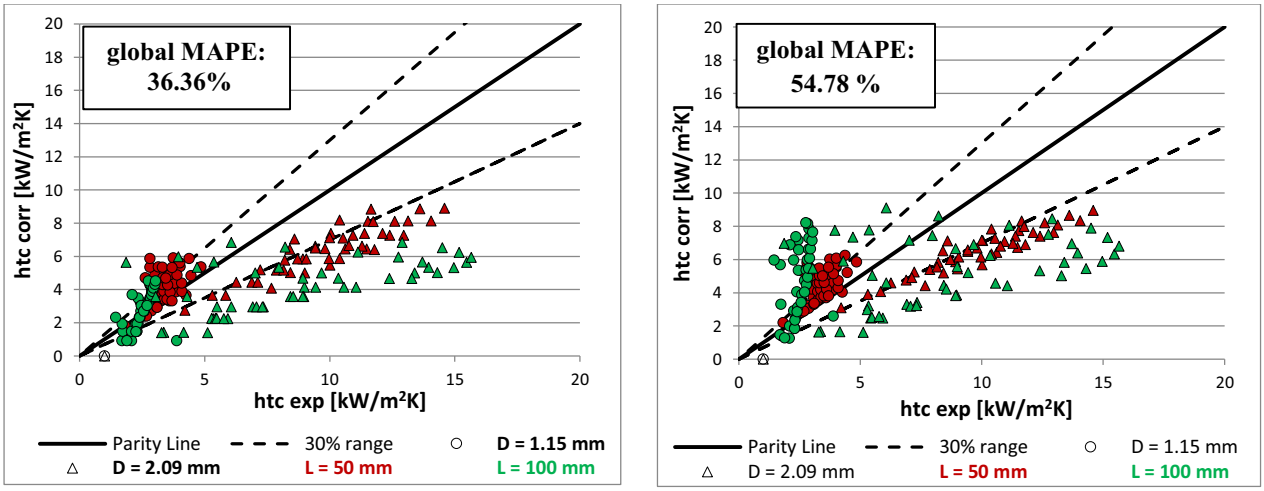

(a): Cooper (b): Bertsch et al.

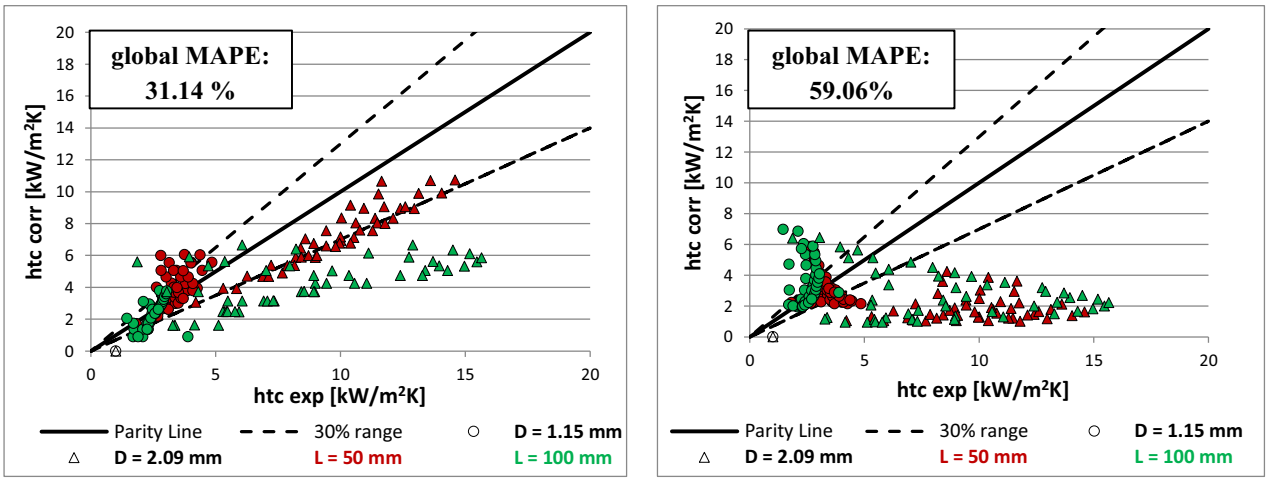

(c): Tran et al. (d): Warrier et al.

Figure 5. Parity plot diagrams for some of the selected correlations

Table 2. Calculated Mean Absolute Percent Error for the selected correlations.

Tested correlation	*E50* *L/D = 43.48*	*E50-2* *L/D = 23.92*	*A100* *L/D = 47.85*	*A100-2* *L/D = 86.96*
Cooper [7]	26.26 %	35.22 %	54.65 %	29.33 %
Bertsch et al. [8]	32.48 %	33.55 %	52.20 %	100.91 %
Li and Wu [9]	72.80 %	18.93 %	36.67 %	87.61 %
Lazarek and Black [10]	175.94 %	21.14 %	42.54 %	153.18 %
Lee and Mudawar [11]	390.88 %	59.70 %	77.35 %	110.59 %
Mahmoud and Karayiannis 2 [12]	44.53 %	31.19 %	57.36 %	192.41 %
Tran et al. [13]	23.96 %	27.32 %	53.15 %	20.12 %
Warrier et al. [14]	31.26 %	80.50 %	72.19 %	52.32 %

8. Conclusions

This paper provides an experimental evaluation of the heat transfer coefficient in multichannel evaporators with three-sides-heated channels, using the fin heat transfer model to consider the unevenness of the heat flux over the vertical walls of the channels. The results showed the following main aspects:

- Smaller channels have lower "fluid-to-wall" heat transfer coefficients, decreasing with the quality;
- Three stages of boiling can be identified: a nucleation-dominated one; an intermediate one; a film forced-convective one. The htc profiles are similar to those studied by Cheng et al. in [6];
- In all the cases heat transfer coefficient increases with the pressure and with the mass flux;
- The Tran correlation and the Cooper's one give the best results, especially for smaller channels, this confirms the strong influence of the nucleate boiling contribution, which is proportional to $q''^{0.6\div0.7}$.
- The Li and Wu correlation gives good results only for 2.09 mm diameter, giving the lowest MAPE (of 18.9%) for the evaporator with a diameter of 2.09 mm and a channel's length of 50 mm. This is probably due to aspect ratio (closer to 1) which is more representative of the dataset used for the correlation development.

Flow instability and unequal flow distribution in lateral channels represents the main criticality in predicting the overall thermal resistance of the evaporator. The temperature distribution in vertical channel walls should be better investigated to develop more accurate models, especially for high aspect ratio micro-channels with adiabatic top side, where the wall heat flux is progressively reduced as the distance from the

base increases and the heat transfer coefficient on vertical walls can strongly differ from that at the channel's base.

9. References

[1] Karayiannis T, & Mahmoud M M (2017). Flow boiling in microchannels: Fundamentals and applications. *Applied Thermal Engineering*, 115, 1372-1397
[2] Yang B, Wang P, & Bar-Cohen A (2007). Mini-contact enhanced thermoelectric cooling of hotspots in high power devices. *IEEE Trans.Compon. Packag. Technol.* , 3(30), 432-438
[3] Criscuolo G, Markussen W B, Meyer K E, & Kaern M R (2022). High heat flux flow boiling of R1234yf, R1234ze(E) and R134a in high aspect ratio microchannels. *International Journal of Heat and Mass Transfer*.
[4] Gugliermetti L, Caruso G, Saraceno L., Zummo G, & Celata G. (2016). Saturated flow boiling of FC-72 in 1mm diameter tube. *International Communications in Heat and Mass Transfer*(75), 115-123.
[5] NIST (s.d.). Reference Fluid Thermodynamic and Transport Properties Database. (REFPROP Version 10) Tratto da https://www.nist.gov/srd/refprop
[6] Cheng L, & Xia G (2017). Fundamental issues, mechanisms and models of flow boiling heat transfer in microscale channels. *International Journal of Heat and Mass Transfer*(108), 97-127.
[7] Cooper M (1984). Heat Flow Rates in Saturated Nucleate Pool Boiling - A Wide -Ranging Examination Using Reduced Properties. *Advances in Heat Transfer*, 16, 157-239.
[8] Bertsch S, Groll E, & Garimella, S (2009). A composite heat transfer correlation for saturated flow boiling in small channels. *International Journal of Heat Mass Transfer*.
[9] Li W, Wu Z (2010). A general correlation for evaporative heat transfer in micro/mini-channels. *International Journal of Heat & Mass Transfer*(53), 1778-1787.
[10] Lazarek G M, Black S H (1982). Evaporative heat transfer pressure drop and critical heat flux in a small vertical tube with R-113. *International Journal of Thermal Science*, 7(25), 945-960.
[11] Lee J, & Mudawar I (2005). Two-phase flow in high heat flux microchannel heat sink for refrigeration cooling applications: Part II-heat transfer characteristics. *International Journal of Heat & Mass Transfer*(48), 941-955.
[12] Mahmoud M, Karayiannis T G (2013). Heat transfer correlation for flow boiling in small to micro tubes. *International Journal of Heat & Mass Transfer*(66), 553-574.
[13] Tran T N, Wambsganss M, & D M France (1996). Small circular and rectangular channel boiling with two refrigerants. *International Journal of Multiphase Flow*, 3(22), 485-498.
[14] Warrier G R, Dhir V K, & Momomda L (2002). Heat transfer and pressure drop in narrow rectangular channels. *Experimental Thermal and Fluid Science*(24), 53-64.